

Miniaturized chip calorimeter for high-pressure cells at low temperature

Neha Kondedan^a, Andreas Rydh^a

^aDepartment of Physics, Stockholm University, Albanova University Center, SE-106 91 Stockholm, Sweden

Abstract

Heat capacity measurements under high pressure places high demands on the calorimeter. Here we describe the development of a miniaturized nanocalorimeter for high-pressure heat capacity measurements at low temperature. The device, fabricated on a silicon substrate, employs a high-frequency AC calorimetry technique and features a design with an outer diameter of 300 μm and thickness of 25-40 μm , small enough to fit into high pressure diamond anvil cells. Miniaturization is achieved by stacking all components, including thermometer and heaters, within a central area. The thin-film calorimeter thermometer measures 40 μm^2 and maintains the sensitivity and properties of larger thermometers. The fabrication process uses controlled anisotropic etch to produce calorimeter chips with a balance between robustness and thickness, suitable for experiments at high pressures and low temperatures. The calorimeter operates at a relatively high characteristic frequency between 10 Hz and 1 kHz, constraining the thermal oscillation to an effective volume dominated by the sample, thereby avoiding the use of a suspended membrane that is the basis for conventional nanocalorimeters.

Keywords: Calorimetry, High pressure, Thin-film thermometry, Frequency dependence, Anisotropic etch

1. Introduction

Specific heat is a crucial thermodynamic quantity for characterizing fundamental material properties and related phase transitions with respect to external conditions, such as magnetic field or pressure. Low-temperature specific heat measurements are particularly useful for understanding superconducting, magnetic, and structural transitions. The advent of AC calorimetry [1] and the development of various types of nanocalorimeters [2, 3, 4] have enabled specific heat measurements on samples down to the nanogram range. Thin-film nanocalorimeters have substantially reduced background heat capacity, but also opened for new measurement possibilities [5, 6, 7, 8, 9].

There are various types of miniaturized calorimeters based on suspended mm^2 membranes combined with advanced microfabrication techniques. For substrate, some calorimeters are fabricated on 2-10 μm thick silicon substrates, taking advantage of the low heat capacity of silicon at low temperatures [10]. Others are constructed on an insulating polymer (poly-para-xylylene) with a copper frame [11, 12]. Most calorimeters are based on SiN_x membranes [13, 14, 15, 16]. The critical component for the miniaturization is the thermometer. Some devices rely on thin-film thermocouples (mainly doped Si) [14], while most are resistive thin-film thermometers based on Pt [15, 13], NbN [12, 17], NbSi [15, 13], AuGe [18, 16], or, recently, NiCrSiO_x [19].

Introducing high pressure to heat capacity measurements, especially at low temperatures, is of great interest because pressure directly affects the electronic density of states through the volume change, and can stabilize new phases and electronic

states [20]. However, high-pressure calorimetry remains a relatively unexplored area due to the significant experimental challenges associated with the integration of calorimeter and pressure cell. Diamond anvil cells are particularly desirable due to their ability to reach extremely high pressures [21, 22]. But, while high-pressure cells in general, and diamond anvil cells in particular, require a small sample, such samples would need even smaller thermometers and heaters to not dominate the total measured heat capacity, thus excluding conventional adiabatic calorimeters. For particular measurement ranges and samples, miniaturized calorimeters based on bare-chip thermometers or thermocouples, either inside or outside the pressure cell, have been devised [23, 24, 25, 26, 27, 28, 29, 30, 31, 32, 33, 34, 35, 36]. A high-pressure calorimeter for general use working over a broad temperature range and in magnetic fields is, to our knowledge, still missing.

Here, we report the fabrication and characterization of a ultra-miniaturized thin-film calorimeter on a silicon chip, that can be easily adapted to various high-pressure cells and cryostats. A key aspect of the fabrication process is the miniaturization of the thermometer while preserving its functional properties.

2. Calorimeter fabrication

2.1. Calorimeter design

The nanocalorimeters are built on a 4-inch silicon wafer with a thickness of $525 \pm 20 \mu\text{m}$, coated with a 1 μm thick SiO_2 layer on both sides, by a batch fabrication process. Over 1600 devices can be fabricated on a single wafer. After depositing all layers, the calorimeters are divided into small chips through front and backside etching. The calorimeter consists of layers of thin-film

Email address: andreas.rydh@fysik.su.se (Andreas Rydh)

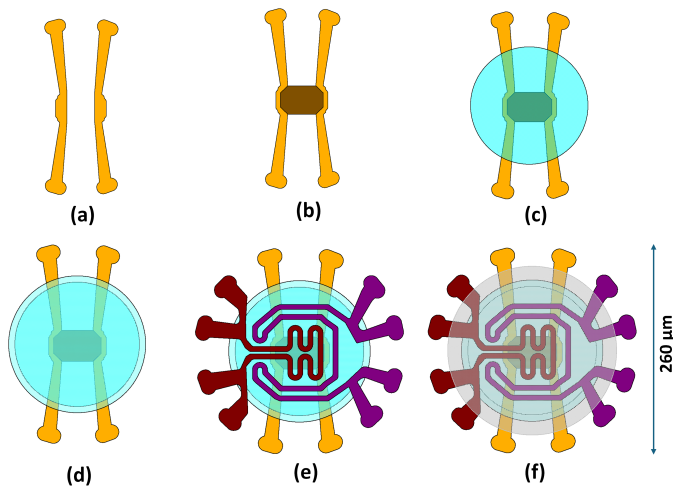


Figure 1: Schematic of the calorimeter layers in the order of deposition. (a) Thermometer leads (b) Thermometer (c) First insulation layer (d) Second insulation layer (e) AC (dark brown) and offset (dark purple) heaters (f) Final insulation layer.

thermometer, AC heater, and offset heater with a double layer of electrical insulation between the active layers. Figure 1 shows the schematic of the calorimeter layers in the order of deposition. The AC heater is a meander-shaped resistor that covers the central area of the calorimeter to ensure uniform heat flow to the sample. It applies an oscillating current that induces temperature oscillations in the sample. The temperature modulated region has an area of approximately $50 \mu\text{m}$ diameter, enabling specific heat measurements of samples with corresponding size. The offset heater lies around the central area. It is supplied with a DC current, which locally raises the temperature of the sample. The double insulation layer avoids pinholes between layers and eliminates step-coverage issues. The low thermal mass of the calorimeter stack ensures a comparatively small contribution to the addenda heat capacity even for a small sample that should ideally cover the thermometer and AC heater, particularly at low temperatures.

2.2. Frontside fabrication

Fabrication of each layer is done by photolithography, thin-film deposition by sputtering and e-beam evaporation, oxygen ashing, and double-layer lift-off. The thermometer is a $40 \mu\text{m} \times 40 \mu\text{m}$ square resistor of thickness 65 nm. It is deposited onto a pair of leads composed of 20 nm Cr and 40 nm Au deposited using e-beam evaporation. The thermometer material is a mixture of a metal with short electronic mean free path and an insulating oxide, produced by co-sputtering NiCr and SiO_2 in an argon and oxygen atmosphere [19]. Following the deposition, a 25 nm thick SiO_2 film is sputtered without breaking the vacuum to prevent the thermometer material from reacting further with the atmosphere. This thin-film thermometer, in direct contact with the sample, provides high sensitivity across a wide temperature range and offers a rapid thermal response. The room temperature resistance of the thermometer can be tuned between 1200–2200 Ω to achieve the desired properties.

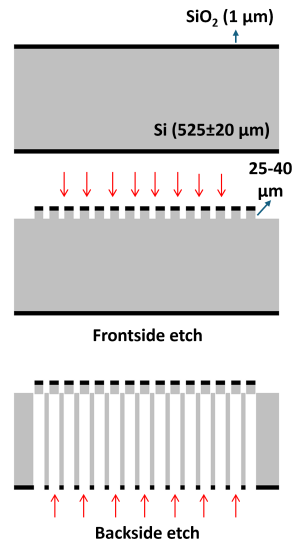


Figure 2: Schematic illustrating the etch steps, showing the full wafer, frontside etch, followed by backside etch. Red arrows indicate the direction of the plasma.

Both heaters are made of 80 nm thick Cr, deposited in a single fabrication step. Careful mask alignment with the thermometer layer is needed to avoid overlap with sharp steps of the combined layer of thermometer and thermometer leads.

SiO_2 is used for the double-insulation layer, which is sputtered in two steps, with each layer having a thickness of 55 nm, as shown in Fig. 1c and d. The layers are covered by a thick SiO_2 layer from the top as a final step (Fig. 1f). The thickness of each layer is chosen to reach full step-coverage of previous layers and to ensure that all edges have sufficiently thick insulation barriers to subsequent layers.

2.3. Etching

The devices are separated into individual calorimeter chips through a dry etch process after frontside fabrication. The 525 μm thick silicon wafer undergoes anisotropic Bosch etch from both front and backside, resulting in thin calorimeter chips with diameters of 300 μm and thicknesses ranging from 25 to 40 μm . The schematic of the etch process is illustrated in Fig. 2.

The 4-inch wafer is initially etched from the frontside, followed by backside etch. For the frontside etch, a photoresist etch mask is created to cover the devices, leaving a circular ring around them. The SiO_2 on top is anisotropically etched at a rate of 400 nm/min. This is followed by Bosch etch of silicon to a depth of up to 40 μm , with a rate of 0.9 $\mu\text{m}/\text{cycle}$, each cycle taking 7 s. The etched depth is measured under a microscope by adjusting the focus. Figure 3a shows the device after frontside etch with the focus on the top surface.

The backside etch mask is a 100 nm thick Cr film created through e-beam evaporation with subsequent lift-off in acetone, prepared before the frontside etch. Chromium is selected for its lower etch rate compared to silicon. The backside mask covers the entire wafer except for discs of 800 μm diameter centered around the devices. For the backside etch, the frontside of the

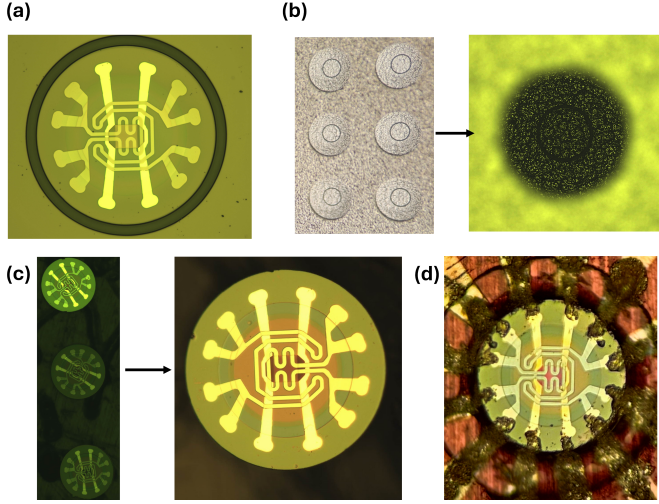


Figure 3: Results after etching from both sides. (a) Frontside mask featuring a ring around the device, which is etched through. (b) Backside of the wafer (zoomed view) after backside etch. The rings around the devices are visible which means the devices are separated. (c) Calorimeter chips after cleaning and separation. Magnified view of one chip is shown on the right side. (d) Calorimeter contact pads connected to external electrical leads using silver epoxy.

wafer is attached to a standard dicing tape (Blue Tack Roll from Semiconductor Equipment Corp.), to hold the final calorimeter chips. The process is otherwise similar to the frontside etch. After etching the SiO_2 covering, the silicon is etched until the ring around the device becomes visible, as shown in Fig. 3b. The process is halted once all the rings are clearly visible. A small variation in thickness could be expected due to variations in etch rate depending on the location on the wafer. After the etch process, the calorimeter chips, shown in Fig. 3c, can be collected and cleaned.

2.4. Electrical connections

The resistance of each active element is measured using the four-probe method, which eliminates contact resistance and contributions from the leads. The contact pads of the active layers, 12 in total, each have a width of $30 \mu\text{m}$ and can be connected to external electrical contacts using a conductive epoxy, either by hand or with a micro-manipulator, as depicted in Fig. 3d. The sidewall of the chip is insulated by melted crystal bond before making electrical contacts. The calorimeter chip is most easily integrated into a high-pressure cell using a split-gasket approach [37], but could also be connected to leads that are directly deposited onto the diamonds [38, 39, 40] or by other means.

3. Thermometer characteristics

The NiCrSiO_x thermometers used here are based on the thin-film thermometers [19] designed to replace the AuGe thermometers used previously in our membrane-based nanocalorimeters [16]. A reduction of the thermometer size

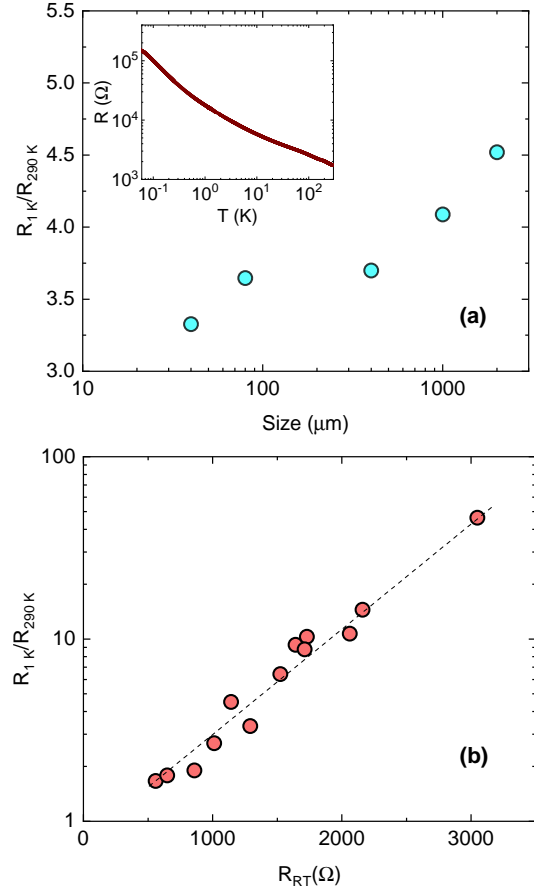


Figure 4: (a) Variation of resistance ratio between 1 K and 290 K with respect to the thermometer size, for thermometers fabricated in the same deposition run. The inset shows the temperature-dependent resistance of a thermometer having a room-temperature resistivity of $10^{-4} \Omega\text{m}$. (b) The resistance ratio between 1 K and 290 K for different $40 \mu\text{m}$ thermometers as a function of corresponding room temperature resistance.

from the $80 \mu\text{m}$ used earlier is needed to fit the active layers into the miniaturized calorimeter. The optimal size of the thermometer depends on several factors. A large thermometer will require a correspondingly large heater to maintain temperature uniformity. A large heater requires a large sample to addenda ratio and increases the heater power, which may be problematic at cryogenic temperatures. However, if the thermometer is very small, self-heating would become a significant problem at the lowest temperatures. The thermometer properties may also be affected by the thermometer leads and film uniformity.

To investigate the impact of size on thermometer characteristics, thermometers with a size ranging from 40 to $2000 \mu\text{m}$ were fabricated under identical conditions. These thermometers exhibit square resistance at room temperature that vary within a range of 100Ω , and they show a resistance value that increases with decreasing temperature, as shown in the inset of Fig. 4a. These thermometers have been calibrated following the method described in [19].

Figure 4a illustrates the relationship between thermometer size and the ratio of thermometer resistance from 1 K to 290 K. The ratio decreases slightly as the size is reduced, but the sensitivity remains largely unaffected. The slight variation in the ratio between different sizes of thermometers could be attributed to the re-sputtering of gold from the leads into the thermometer region, particularly along the edges during thermometer deposition. This process results in a tendency to become slightly more metallic. This effect is more pronounced in smaller thermometers, resulting in a lower resistance ratio for given deposition conditions.

Figure 4b shows the low-temperature sensitivity of several 40 μm thermometers as a function of room temperature resistance, with the variation of properties obtained by tuning the metal to insulator deposition conditions. The resistance ratio shows a nearly exponential increase with room temperature resistance, allowing for predictable low-temperature characteristics of the 40 μm thermometer, similar to those observed in the 80 μm thermometers [19]. This confirms that miniaturizing the thermometer dimensions does not significantly alter the functional properties of the thermometers.

4. Heat-flow analysis

The heat flow of the calorimeter system can be modeled as a one-dimensional heat diffusion problem by approximating the planar AC heater geometry illustrated in Fig. 5a as a 1D wire with a point heat source of Fig. 5b. In a wire, the heat wave propagates along the wire (in the r direction) from the point heat source. In the calorimeter system, although heat is transmitted in multiple directions, as indicated by the red arrows in the Fig. 5a, the primary region of interest for heat propagation from the heater area is up and down, enclosed by the dotted blue box in the figure, which includes the sample and a portion of the silicon substrate.

The AC heater generates a modulated heat wave, which transfers heat to both the sample and the silicon substrate. The extent of the thermal wave is determined by the angular frequency ω of the temperature oscillation. In the 1D model, temperature modulation as a function of distance (r) is given by [41]

$$T_{ac}(r) \propto \frac{1}{\omega} \exp(-kr - ikr - i\pi/2), \quad (1)$$

where the decay constant k is the inverse of the thermal diffusion length l_{th} . Equation (1) is valid under the condition that $\omega\tau_e \gg 1$, where τ_e is the relaxation time between the system and the thermal bath.

The thermal diffusion length l_{th} can be estimated within the pseudo-one-dimensional geometry, and is given by

$$l_{th}(\omega) = \sqrt{\frac{2D}{\omega}}. \quad (2)$$

Here, D is the diffusivity of the material, defined as

$$D = \frac{K}{\rho c_p}, \quad (3)$$

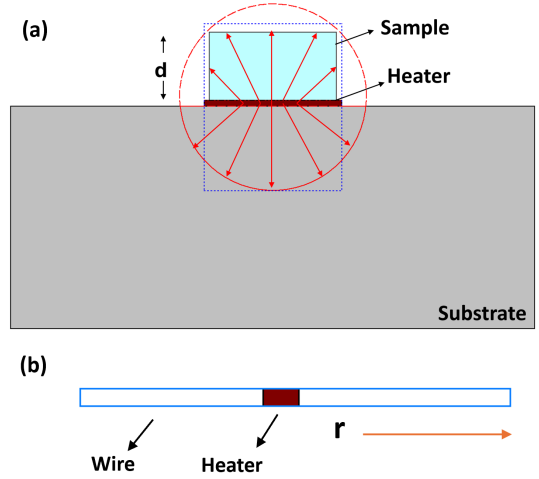


Figure 5: Schematic of the calorimeter with a sample on top. The red arrows depict the direction of heat flow from the heater, while the red circle indicates the extent of diffusion (l_{th}). The dotted blue box highlights the volume that is temperature modulated in the 1D diffusion model. (b) Illustration of a thin wire with a heat source located at a single point, where oscillations propagate along the r direction.

where K , ρ , and c_p represent thermal conductivity, volume density, and specific heat respectively. For uniform heating within the sample, the sample thickness d must be much smaller than l_{th} . Otherwise, a thermal gradient will develop in the sample perpendicular to the planar heat source. Beyond the range of the thermal diffusion length ($r \gg l_{th}$), the temperature oscillation is negligible and the substrate (including possible pressure medium) acts as the thermal bath.

The diffusion introduces a frequency-dependent heat capacity, $C = C(\omega)$ that is probed. To accurately measure the sample heat capacity, additional addenda heat capacity must be minimized and the full sample heat capacity must be included. This optimization is non-trivial and depends on the properties of the sample, substrate, and pressure medium. By adjusting the thermal diffusion length through the frequency, using Eq. (2), the thermal oscillation should be restricted to a volume that extends only slightly beyond the sample. The relative contributions from sample and substrate to the probed heat capacity then depends on their effusivities $e = (K\rho c_p)^{1/2}$, since the heater area A_{heat} defines a probed volume $l_{th}A_{heat}$ on each side of the heater so that the participating heat capacity is given by $l_{th}A_{heat}\rho c_p \propto e$. Thus, when the sample effusivity exceeds that of the substrate, a relatively small substrate addenda will be probed, leaving the sample heat capacity well defined. Similarly to the effusivity of the calorimeter substrate, the effusivity of the pressure medium should be kept as low as possible, to restrict the thermal wave from extending beyond the top surface of the sample. This is normally the case, since most pressure media are insulators with low effusivities. In this case, the thermal oscillation is localized well to the sample and some part of the substrate. Since the thermal wave never reaches the metallic pressure cell gasket, the probed volume remains small and well defined, representing the sample heat capacity with a frequency dependent back-

ground from the silicon substrate.

5. Calorimeter performance

5.1. Frequency and temperature dependence

The empty calorimeter was characterized from room temperature to below 1 K. A $0.77\ \mu\text{g}$ $\text{Gd}_2\text{Zn}_{17}$ crystal with an antiferromagnetic transition at 9 K [42] was also used as a test sample, mounted on the calorimeter using a micromanipulator with a tiny droplet of Apiezon-N grease for thermal attachment. Figure 6a shows the temperature oscillation amplitude of the empty calorimeter (red curves) and calorimeter with sample (blue curves) at different temperatures, as a function of frequency. From the figure, one can see that the temperature oscillation is significantly reduced by the presence of the sample, indicating that the sample heat capacity acts to reduce the thermal oscillation.

Analyzing the frequency dependence of Fig. 6a, three different frequency regimes can be identified for each curve. At low frequency, the temperature oscillation amplitude is constant (at 1 K) or slightly decreasing (at 10 K and 30 K) with frequency. This behavior corresponds to the low-frequency regime of regular ac calorimetry, where the effective thermal link K_{eff} is probed and there is no effect from the sample heat capacity on the temperature oscillation; $T_{\text{ac}} \approx P_{\text{ac}}/K_{\text{eff}}$. In this regime the phase between temperature oscillation and applied power P_{ac} is small.

At intermediate frequencies, the temperature oscillation starts to drop quickly with frequency, indicating that the heat capacity reduces the temperature oscillation. For a well-defined heat capacity C_{eff} , the relation between C_{eff} and T_{ac} is given by [16]

$$C_{\text{eff}} = \frac{P_{\text{ac}}}{\omega T_{\text{ac}}} \sin \varphi, \quad (4)$$

where φ is the phase between applied power and temperature oscillation. Since the calorimeter contribution to the heat capacity will be frequency dependent, it is not trivial to acquire absolute accurate measurements of the sample heat capacity $C_s = C_{\text{eff}}(\omega) - C_{\text{cal}}(\omega)$.

Going to the highest frequency range, the effective sample heat capacity will start to decrease due to the thermal length becoming shorter than the sample thickness. In this range, $\tan \varphi = \omega C_{\text{eff}}/K_{\text{eff}}$ is no longer proportional to ω , but starts to quickly decrease with increasing frequency with a concurrent increase of $K_{\text{eff}}(\omega)$ and decrease of $C_{\text{eff}}(\omega)$. There is, thus, a maximum in $\tan \varphi$ beyond which absolute accuracy cannot be obtained. The maximum in $\tan \varphi$ depends on the sample heat capacity, sample thermal conductivity, and how well the sample is attached to the calorimeter, but is normally located near $\tan \varphi \approx 1$.

The suitable measurement frequency depends on the requirements on absolute accuracy and resolution. Measurements in the highest frequency range, beyond the maximum in $\tan \varphi$ will give higher resolution (other parameters optimized). As seen in Fig. 6a the ratio of T_{ac} without and with sample at 30 K reaches

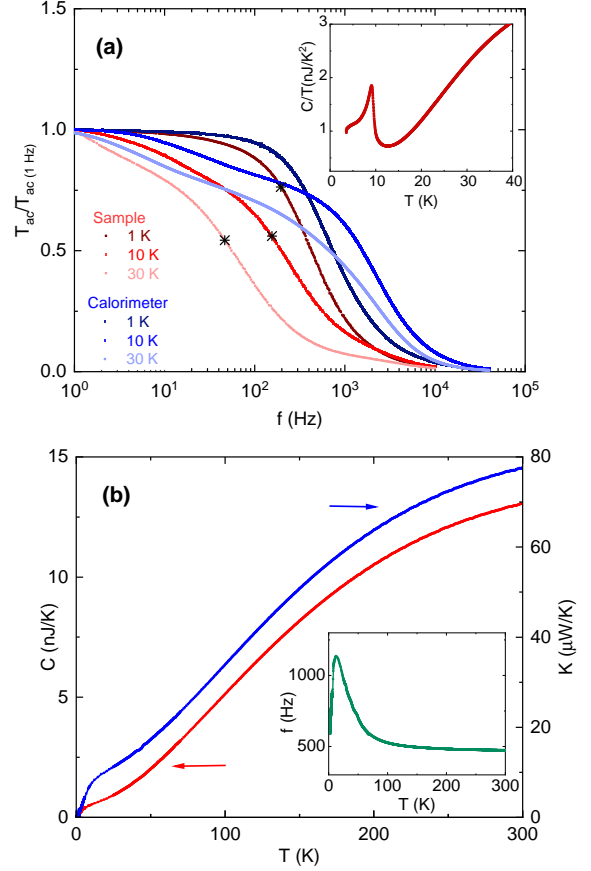


Figure 6: Calorimeter characterization. (a) Frequency dependence of the temperature oscillation amplitude, normalized to oscillation amplitude at 1 Hz, for calorimeter with and without sample, measured at 1 K, 10 K, and 30 K. The inset shows the measured heat capacity, plotted as C/T , as a function of temperature for a $\text{Gd}_2\text{Zn}_{17}$ crystal. The measurement frequency was varied to maintain a constant phase between applied power and temperature oscillation. The corresponding measurement frequencies at 1 K, 10 K, and 30 K are indicated by black markers in the main figure. (b) Thermal conductance and heat capacity of the calorimeter chip, from 0.1 K to 300 K. The inset shows the corresponding frequency during the measurement.

a factor of 6 at 1 kHz, indicating that the probed $C_s(\omega)$ is about 5 times higher than $C_{\text{cal}}(\omega)$ at this frequency. However, measurements at the intermediate frequency range will always include the full C_s (temperature oscillation is uniform in the entire sample), retaining the possibility to obtain absolute accuracy as long as the calorimeter $C_{\text{cal}}(\omega)$ is separately measured.

The inset of Fig. 6a shows the heat capacity of the small $\text{Gd}_2\text{Zn}_{17}$ crystal. The antiferromagnetic ordering transition at 9 K is clearly observed. These measurements were taken with $\tan \varphi = 0.8$. The corresponding locations of the measurement frequencies in the main panel of Fig. 6a are indicated by black markers.

Figure 6b shows the temperature dependence of the calorimeter heat capacity C_{cal} and thermal conductance K_{eff} of the empty calorimeter chip. The temperature dependence of the measurement frequency is shown in the inset. This fre-

quency was obtained by continuously adjusting frequency to obtain $\tan \phi = 1$. The C_{cal} curve gives an indication of the smallest samples that can be studied with the calorimeter. The background corresponds roughly to a 30 ng piece of copper, making it possible to obtain signals from samples down to the few ng range.

5.2. Pressurization in a diamond anvil cell

The calorimeter chips were subjected to high-pressure conditions using a diamond anvil cell with a culet diameter of 1.2 mm. During these tests, the devices were fully immersed in the pressure medium to ensure uniform pressure distribution. In our pressure cell, the devices withstood pressures up to the maximum cell pressure of 2 GPa without failure. This ability to withstand pressure confirms that the chosen calorimeter substrate material survives in high-pressure experiments. The ultimate maximum pressure tolerable by the silicon chips remains to be determined.

6. Summary and conclusions

In summary, we describe a miniaturized chip calorimeter for heat capacity measurements at low temperatures and high pressures. The miniaturization enables the calorimeter to fit into small sample volumes, such as inside high pressure diamond anvil cells combined with cryogenic systems. From an analysis of the frequency dependence of the calorimeter with and without a test sample, we find the suitable measurement conditions, where the sample heat capacity can be separated from the frequency dependent calorimeter background. While the calorimeter is designed for high pressure studies, it could also find its applications for high-frequency measurements of small samples, such as in pulsed magnetic fields.

Acknowledgements

Support from the Knut and Alice Wallenberg Foundation under grant number KAW 2018.0019 and the Swedish Research Council, grant number 2021-04360, are acknowledged. We thank J. Palmer-Fortune, A. Bangura, U. Häussermann, and A. Khansili for insightful discussions on the development of the calorimeter.

References

- [1] P. F. Sullivan, G. Seidel, Steady-state, ac-temperature calorimetry, *Physical Review* 173 (3) (1968) 679.
- [2] J.-L. Garden, O. Bourgeois, Nanocalorimetry, *Encyclopedia of nanotechnology* (2012) 1491–1504.
- [3] F. Yi, D. A. LaVan, Nanocalorimetry: Exploring materials faster and smaller, *Applied Physics Reviews* 6 (3) (2019).
- [4] J.-L. Garden, H. Guillou, A. F. Lopeandia, J. Richard, J.-S. Heron, G. Souche, F. Ong, B. Vianay, O. Bourgeois, Thermodynamics of small systems by nanocalorimetry: From physical to biological nano-objects, *Thermochimica Acta* 492 (1-2) (2009) 16–28.
- [5] A. Khansili, A. Bangura, R. D. McDonald, B. J. Ramshaw, A. Rydh, A. Shekhter, Calorimetric measurement of nuclear spin-lattice relaxation rate in metals, *Physical Review B* 107 (19) (2023) 195145.
- [6] K. Willa, Z. Diao, D. Campanini, U. Welp, R. Divan, M. Hudl, Z. Islam, W.-K. Kwok, A. Rydh, Nanocalorimeter platform for in situ specific heat measurements and x-ray diffraction at low temperature, *Review of scientific instruments* 88 (12) (2017).
- [7] F. Yi, A. Stevanovic, W. A. Osborn, A. Kolmakov, D. A. LaVan, A multi-environment nanocalorimeter with electrical contacts for use in a scanning electron microscope, *Materials horizons* 4 (6) (2017) 1128–1134.
- [8] F. Yi, J. B. DeLisio, M. R. Zachariah, D. A. LaVan, Nanocalorimetry-coupled time-of-flight mass spectrometry: identifying evolved species during high-rate thermal measurements, *Analytical chemistry* 87 (19) (2015) 9740–9744.
- [9] M. Zhang, E. Olson, R. Twesten, J. Wen, L. Allen, I. Robertson, I. Petrov, In situ transmission electron microscopy studies enabled by microelectromechanical system technology, *Journal of materials research* 20 (7) (2005) 1802–1807.
- [10] F. Fominaya, T. Fournier, P. Gandit, J. Chaussy, Nanocalorimeter for high resolution measurements of low temperature heat capacities of thin films and single crystals, *Review of scientific instruments* 68 (11) (1997) 4191–4195.
- [11] O. Bourgeois, C. Macovei, E. André, J.-L. Garden, J. Chaussy, D. Givord, A new sensor for thermodynamic measurements of magnetization reversal in magnetic nanomaterials, *Journal of Magnetism and Magnetic Materials* 316 (2) (2007) e94–e96.
- [12] A. F. Lopeandia, E. André, J.-L. Garden, D. Givord, O. Bourgeois, Highly sensitive parylene membrane-based ac-calorimeter for small mass magnetic samples, *Review of Scientific Instruments* 81 (5) (2010).
- [13] D. Denlinger, E. Abarra, K. Allen, P. Rooney, M. Messer, S. Watson, F. Hellman, Thin film microcalorimeter for heat capacity measurements from 1.5 to 800 K, *Review of Scientific Instruments* 65 (4) (1994) 946–959.
- [14] A. Minakov, S. Roy, Y. V. Bugoslavsky, L. Cohen, Thin-film alternating current nanocalorimeter for low temperatures and high magnetic fields, *Review of Scientific Instruments* 76 (4) (2005).
- [15] D. W. Cooke, K. Michel, F. Hellman, Thermodynamic measurements of submilligram bulk samples using a membrane-based “calorimeter on a chip”, *Review of Scientific Instruments* 79 (5) (2008).
- [16] S. Tagliati, V. M. Krasnov, A. Rydh, Differential membrane-based nanocalorimeter for high-resolution measurements of low-temperature specific heat, *Review of Scientific Instruments* 83 (5) (2012).
- [17] O. Bourgeois, S. Skipetrov, F. Ong, J. Chaussy, Attojoule calorimetry of mesoscopic superconducting loops, *Physical review letters* 94 (5) (2005) 057007.
- [18] W. C. Fon, K. C. Schwab, J. M. Worlock, M. L. Roukes, Nanoscale, phonon-coupled calorimetry with sub-attojoule/kelvin resolution, *Nano letters* 5 (10) (2005) 1968–1971.
- [19] N. Fortune, J. E. Palmer-Fortune, A. Trainer, A. Bangura, N. Kondedan, A. Rydh, Wide-range thin-film ceramic-metal-alloy thermometers with low magnetoresistance, *Physical Review Applied* 20 (5) (2023) 054016.
- [20] A. Hermann, Chemical bonding at high pressure, *Reviews in computational chemistry* 30 (2017) 1–41.
- [21] A. Jayaraman, Diamond anvil cell and high-pressure physical investigations, *Reviews of Modern Physics* 55 (1) (1983) 65.
- [22] A. Jayaraman, Ultrahigh pressures, *Review of Scientific Instruments* 57 (6) (1986) 1013–1031.
- [23] G. Jura, W. Stark Jr, A technique for measurement of the heat capacity of metals under pressure, *Review of Scientific Instruments* 40 (5) (1969) 656–660.
- [24] C. Loriers-Susse, J.-P. Bastide, G. Bäckström, Specific heat measured at high pressures by a pulse method, *Review of Scientific Instruments* 44 (9) (1973) 1344–1349.
- [25] J. Baloga, C. Garland, Ac calorimetry at high pressure, *Review of Scientific Instruments* 48 (2) (1977) 105–110.
- [26] A. Eichler, W. Gey, Method for the determination of the specific heat of metals at low temperatures under high pressures, *Review of Scientific Instruments* 50 (11) (1979) 1445–1452.
- [27] H. Bohn, A. Eichler, Specific heat of d-hcp and fcc lanthanum under high pressure, *Zeitschrift für Physik B Condensed Matter* 83 (1991) 105–111.
- [28] A. Demuer, C. Marcenat, J. Thomasson, R. Calemczuk, B. Salce, P. Lejay, D. Braithwaite, J. Flouquet, Calorimetric study of CeRu₂Ge₂ under continuously swept hydrostatic pressure up to 8 GPa, *Journal of low temperature physics* 120 (2000) 245–257.

- [29] F. Bouquet, Y. Wang, H. Wilhelm, D. Jaccard, A. Junod, Calorimetric investigation of CeRu₂Ge₂ up to 8 GPa, *Solid state communications* 113 (7) (2000) 367–371.
- [30] H. Wilhelm, Ac-calorimetry at high pressure and low temperature, *Advances in Solid State Physics* (2003) 889–913.
- [31] R. Lortz, A. Junod, D. Jaccard, Y. Wang, C. Meingast, T. Masui, S. Tajima, Evolution of the specific-heat anomaly of the high-temperature superconductor YBa₂Cu₃O₇ under the influence of doping through application of pressure up to 10 GPa, *Journal of Physics: Condensed Matter* 17 (26) (2005) 4135.
- [32] O. Kubota, Y. Nakazawa, Construction of a low-temperature thermodynamic measurement system for single crystal of molecular compounds under pressures, *Review of Scientific Instruments* 79 (5) (2008).
- [33] K. Umeo, Alternating current calorimeter for specific heat capacity measurements at temperatures below 10 K and pressures up to 10 GPa, *Review of Scientific Instruments* 87 (6) (2016).
- [34] Z. M. Geballe, V. V. Struzhkin, Ac calorimetry of H₂O at pressures up to 9 GPa in diamond anvil cells, *Journal of Applied Physics* 121 (24) (2017).
- [35] E. Gati, G. Drachuck, L. Xiang, L.-L. Wang, S. L. Bud'ko, P. C. Canfield, Use of cernox thermometers in ac specific heat measurements under pressure, *Review of Scientific Instruments* 90 (2) (2019).
- [36] V. Martelli, H. Rønnow, et al., High-pressure specific heat technique to uncover novel states of quantum matter, *arXiv preprint arXiv:2007.07380* (2020).
- [37] N. Kondedan, U. Häussermann, A. Rydh, Split-gasket approach to the integration of electrical leads into diamond anvil cells, unpublished.
- [38] T. A. Grzybowski, A. L. Ruoff, Band-overlap metallization of BaTe, *Physical review letters* 53 (5) (1984) 489.
- [39] C. Gao, Y. Han, Y. Ma, A. White, H. Liu, J. Luo, M. Li, C. He, A. Hao, X. Huang, et al., Accurate measurements of high pressure resistivity in a diamond anvil cell, *Review of scientific instruments* 76 (8) (2005).
- [40] S. T. Weir, J. Akella, C. Aracne-Ruddle, Y. K. Vohra, S. A. Catledge, Epitaxial diamond encapsulation of metal microprobes for high pressure experiments, *Applied Physics Letters* 77 (21) (2000) 3400–3402.
- [41] I. Hatta, Y. Sasuga, R. Kato, A. Maesono, Thermal diffusivity measurement of thin films by means of an ac calorimetric method, *Review of Scientific Instruments* 56 (8) (1985) 1643–1647.
- [42] C. Marquina, N.-T. Kim-Ngan, K. Buschow, J. Franse, M. Ibarra, Specific heat of Gd₂Zn₁₇ and Yb₂Zn₁₇ intermetallic compounds, *Journal of magnetism and magnetic materials* 157 (1996) 403–404.